Mechanistic Insights on the Enantioselective (4 + 3) Cycloaddition Between Oxyallylcations and Furans Catalyzed by BINOL-Based Phosphoramides

Manuel Pedrón,[a,*] Laura Villar,[b] Uxue Uria,[b] Liher Prieto,[b] Tomas Tejero,[c] Pedro Merino,[a,*] and Jose L. Vicario[b,*]

[a] Instituto de Biocomputación y Física de Sistemas Complejos (BIFI). Universidad de Zaragoza. 5009 Zaragoza (Spain)
   E-mail: manolo@unizar.es; pmerino@unizar.es

[b] Department of Organic and Inorganic Chemistry. University of the Basque Country (UPV/EHU). P.O. Box 644, 48080 Bilbao (Spain).
   Tel: + 34 94 601 5454
   E-mail: joseluis.vicario@ehu.es

[c] Instituto de Síntesis Química y Catálisis Homogénea (ISQCH). Universidad de Zaragoza-CSIC. 5009 Zaragoza (Spain)
   Tel: + 34 87 655 3783

Supporting information for this article is available on the WWW under https://doi.org/10.1002/adsc.202301188

Abstract: The mechanism of the enantioselective (4 + 3) cycloaddition between furan derivatives and oxyallylcations, which are generated from the corresponding oxiranes through in situ oxidation of allenamides, has been studied using DFT methods. The research has revealed that, under acid-catalysis by a chiral non-racemic phosphoramide, the epoxide ring-opening proceeds without any energy barrier, while the rate-limiting step is the electrophilic attack of the intermediate enaminium ion on the furan ring. The reaction exhibits low energy barriers when dealing with furan derivatives unsubstituted at C2 and C5. Calculations predict the formation of an achiral regioisomer for 2-substituted furans, a prediction that has been experimentally confirmed. Additionally, the calculations accurately predict the reaction with substituted allenamides.

Keywords: Cycloadditions; Phosphoramides; Oxyallyl cations; Epoxide opening; DFT
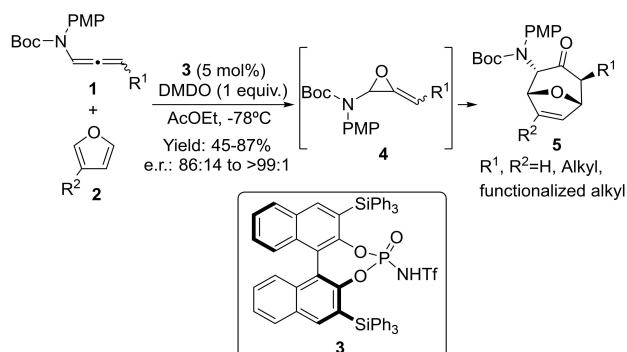
Introduction

Cycloaddition reactions represent one of the most efficient and direct approach for the synthesis of cyclic molecules.[1] This type of transformations not only enable the direct construction of the cyclic target in a single step through the reaction between two components involving the consecutive formation of at least two new C–C or C-heteroatom bonds, but also allow for an exquisite degree of selectivity when generating complex molecular scaffolds with multiple stereogenic centres due to their normally inherent stereospecific and stereoselective nature.[2] In this sense, the venerable Diels-Alder reaction stands as the archetypical example of a cycloaddition reaction that is regarded a one of the most widely employed disconnective tools when planning the synthesis of complex molecules containing six-membered carbo- or heterocycles.[3] As a matter of fact, the chemical literature provides multiple methodologies for performing stereocontrolled (4 + 2)[4] and (3 + 2)[5] cycloaddition reactions that conduct to the formation of five- and six-membered cyclic entities as single stereoisomers in a highly reliable manner. In contrast, the formation of medium-sized seven-membered carbo- or heterocyclic molecules through cycloaddition reaction still represents a challenge by itself due to transannular strain and unfavourable entropic factors involved.[6] In partic-

ular, the stereoselective formation of 7-membered carbocyclic scaffolds through catalytic enantioselective cycloaddition chemistry is typically achieved by means of either $(5+2)$[7] or $(4+3)$[8] cycloadditions, with some very efficient methodologies developed in the chemical literature.

Specifically, the $(4+3)$ cycloaddition reaction between furans and oxyallyl cations[9] has attracted an important deal of attention among the synthetic community, as it represents a direct approach to the 8-oxabicyclo[3.2.1]octane scaffold, that is present in a wide variety of biologically relevant natural products.[10] Despite the intensive efforts in this field, methods for performing this transformation in an enantioselective manner are still very limited and poorly developed. After the initial pioneering report by Harmata in 2003 and Hsung in 2005,[11] actually only a few other reports have been published that involve either the use of transition metal catalysis[12] or moving to organocatalysis as the methodological tool to achieve enantiocontrol.[13]

In this particular context, some time ago we reported that *in situ* generated oxyallyl cations react with furans **2** to provide $(4+3)$ cycloaddition products **5** as highly enantioenriched materials when the reaction is carried out using BINOL-based chiral *N*-trifluoromethanesulfonamide **3** as catalyst (Scheme 1).[13c] The key oxyallyl cations were also formed in the reaction medium through the Brønsted acid-catalyzed-ring opening of alkylideneoxiranes, which were also generated *in situ* by chemoselective oxidation of allenamides **1**, following the reaction design reported by Hsung in his seminal work.[11] A remarkable feature of this reaction is the fact that both terminally unsubstituted and substituted allenamides **1** react efficiently in this transformation, highlighting the fact that substituted allenamides provide typically better levels of enantioselectivity than unsubstituted ones. This stands in contrast with reported methodologies[13] in which unsubstituted allenamides **1** ($R^1 = H$) perform significantly more efficiently in terms

of stereocontrol. It is important to note that these terminally substituted allenamides are chiral compounds that are employed as racemic materials, as the stereochemical information is deleted upon formation of the oxyallyl cation intermediate.

With this information in mind, we decided to carry out further investigations in order to gain further insights into the mechanism of this reaction and, especially, the activation mode and origin of enantiocontrol provided by the phosphoramide catalyst. For this purpose, we settled on implementing a series of computational studies to elucidate the reaction pathway together with several experimental studies and control reactions that could support the computational data.

Results and Discussion

We studied computationally the transformation of epoxide **4** formed *in situ* into final adduct **5**. Geometry full optimizations were made at ωB97X-D/def2SVP level considering solvent effects (EtOAc) using the PCM model. Single point calculations using def2TZVP basis set and also considering solvent effects (PCM, EtOAc) were carried out over optimized geometries to obtain the energy values. We considered a simple but chiral model of the catalyst **3** (**CAT-H**) with the real substrates. This approach let us to consider enantioselectivity from the first moment studying the real reaction. A catalytic cycle for the entire transformation can be proposed (Scheme 2) in which three stages are differentiated: a) ring-opening of the allenyl epoxide;
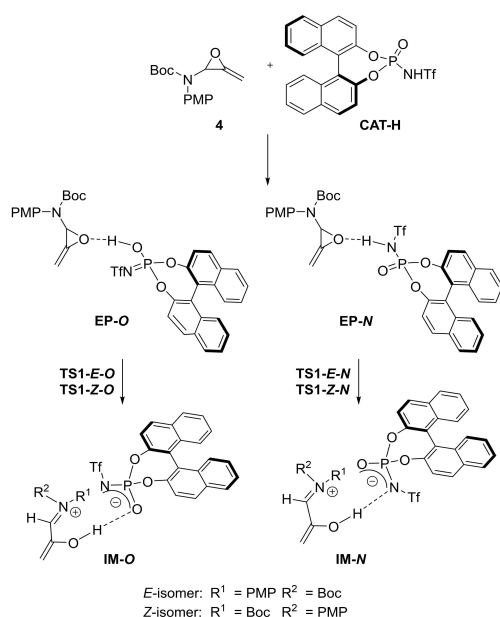

Scheme 1. Enantioselective oxidative $(4+3)$ cycloadditions between allenamides and furans
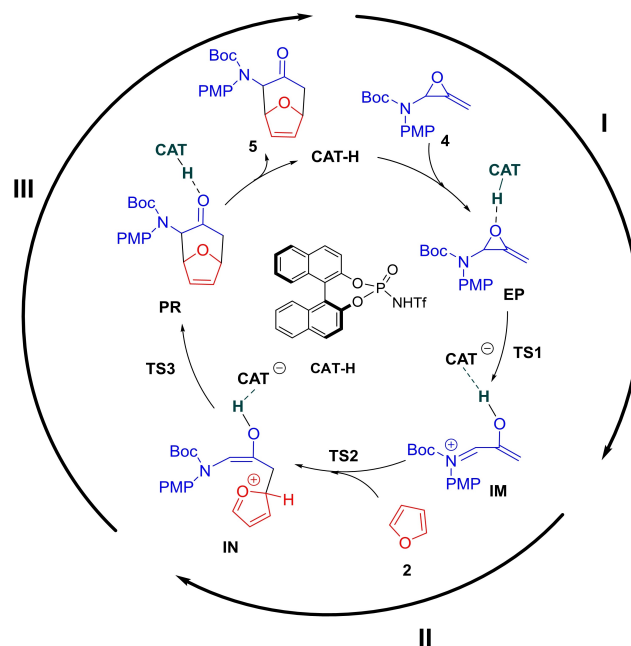
Scheme 2. Proposed catalytic cycle.

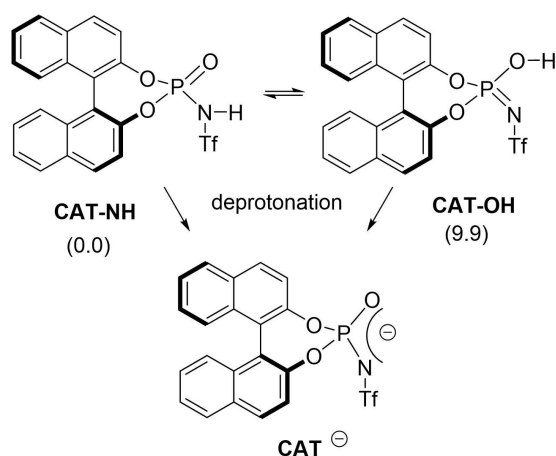b) reaction with furan and c) formation of the final product.

Ring-Opening of Allenyl Epoxide (I)

Coordination of the catalyst to the oxirane ring promotes the ring-opening to give an oxy-eniminium that can be formed as *Z* or *E* isomers, each of one could adopt a *s-cis* or *s-trans* conformation.

Due to the tautomeric equilibrium in the catalyst, there are two possible coordination modes with substrates (See Scheme 3 for details). Both coordinated species, **EP-O** and **EP-N**, actually exist in equilibrium

due to the tautomerism of the P(O)NHTf moiety on the catalyst (Scheme 4).

The energetic difference between the NH- and OH-forms is 9.9 kcal/mol in favour of the NH form, which renders the presence of the OH tautomer negligible (the corresponding transition structure would have a minimum value of ca. 10 kcal/mol). However, we considered both coordination modes for subsequent reactions because **IM-O** and **IM-N** represent two forms of a single species capable of coordinating with two different centers of the catalyst, leading to two distinct geometries that require separate computational treatments. Consequently, we located four transition structures corresponding to the formation of *E* and *Z* isomers under the two coordination modes rendering four intermediates **IM** (Figure 1).

The preferred transition structure obtained was the one that led to an intermediate with (*E*)-configuration of the iminium moiety and *O*-coordinated to the catalyst. Coordination through the nitrogen was only 1.9 kcal/mol higher in energy. Those transition struc-

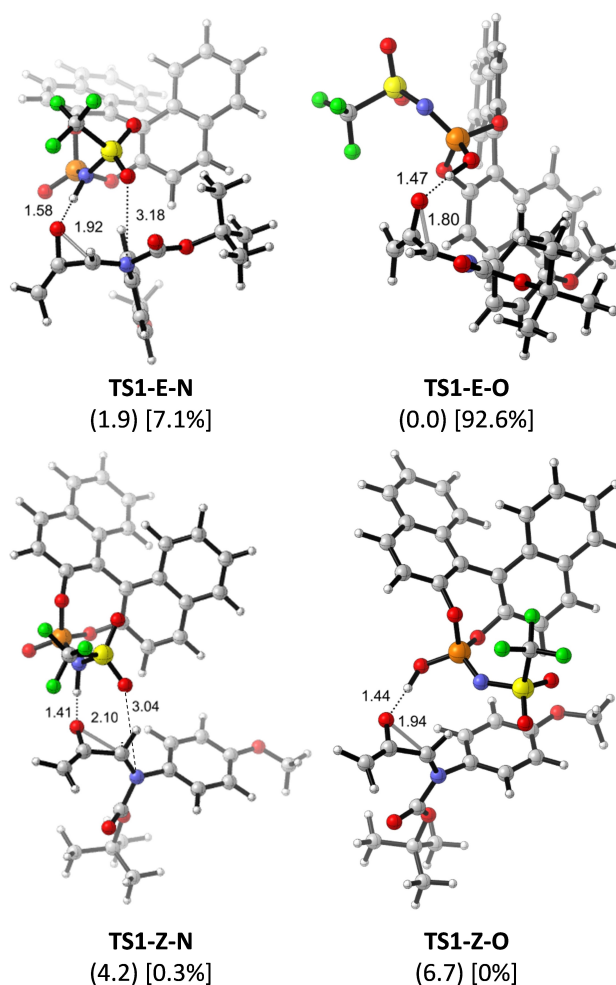**Scheme 3.** Ring-opening of the allenyl epoxide. Only *s-trans* conformers are shown for **IM**.

Scheme 4. Tautomerism of the catalyst. Numbers between brackets represent the difference in stability in kcal/mol.

Figure 1. Optimized transition structures corresponding to the ring-opening of the allenyl epoxide.

Adv. Synth. Catal. **2023**, *365*, 1–10   **Wiley Online Library**   3

These are not the final page numbers! ↗↗

tures leading to a (*Z*)-iminium ion were too high in energy to be considered. In addition to the H-bond interaction with the oxygen atom of the epoxide, an additional interaction with the catalyst was detected as we had initially suggested. For instance, in the case of *N*-coordinated species, the S=O group of the triflate is positioned at 3.04 (**TS1-Z-N**) and 3.18 (**TS1-E-N**) Å away from the iminium nitrogen atom, suggesting some electrostatic interaction. Despite this observation, the *O*-coordinated transition structures, which do not exhibit such interactions, were found to be more stable, primarily due to steric reasons. This leads to the idea that additional electrostatic interactions can be disregarded. In general, the lack of planarity of the *p*-methoxyphenyl group with the iminium ion moiety, along with the bulkiness of the *tert*-butoxycarbonyl group, creates enough steric hindrance to prevent the iminium nitrogen atom and the phosphoramide group from placing in close proximity.

The starting complexes can interconvert since the obtention of *E* or *Z* iminium ion isomers depends on the conformation of the C–N bond. Those complexes corresponding to a conformation leading to an (*E*)-iminium ion intermediate were found to be the most stable situations, with a negligible difference of 0.2 kcal/mol. In all cases, the *s-cis* conformers were formed as a consequence of the anchimeric assistance of the nitrogen lone pair which forces the oxygen to be placed opposite to the nitrogen (Scheme 5).

However, these *s-cis* conformers resulted to be less stable than their corresponding *s-trans* conformers. As a result, we considered the occurrence of a conformational equilibrium after the ring-opening event and therefore only the *s-trans* conformers were taken into consideration for studying the next step. The ultimate energy barrier for this step of the reaction, starting from allenyl epoxide **4** and ending in the eniminium ion intermediate **IM** was found to be only 0.2 kcal/mol. (Figure 2).

Both starting materials (**RE**) and final intermediates (**IM**) can interconvert between each other as indicated for the former case, due to the above mentioned lability of the geometry of the iminium ion and the interconversion of the *N* and *O*-coordination.

Scheme 5. Obtention of *s-cis* conformers.

Reaction with the Furan Ring (II)

The reaction between oxy eniminium ions **IM** and furan to give the chiral intermediate carbocation **IN** was then approached (Scheme 6).

As mentioned before, out of the two possible conformations, s-*cis* and s-*trans* of **IM**, we only
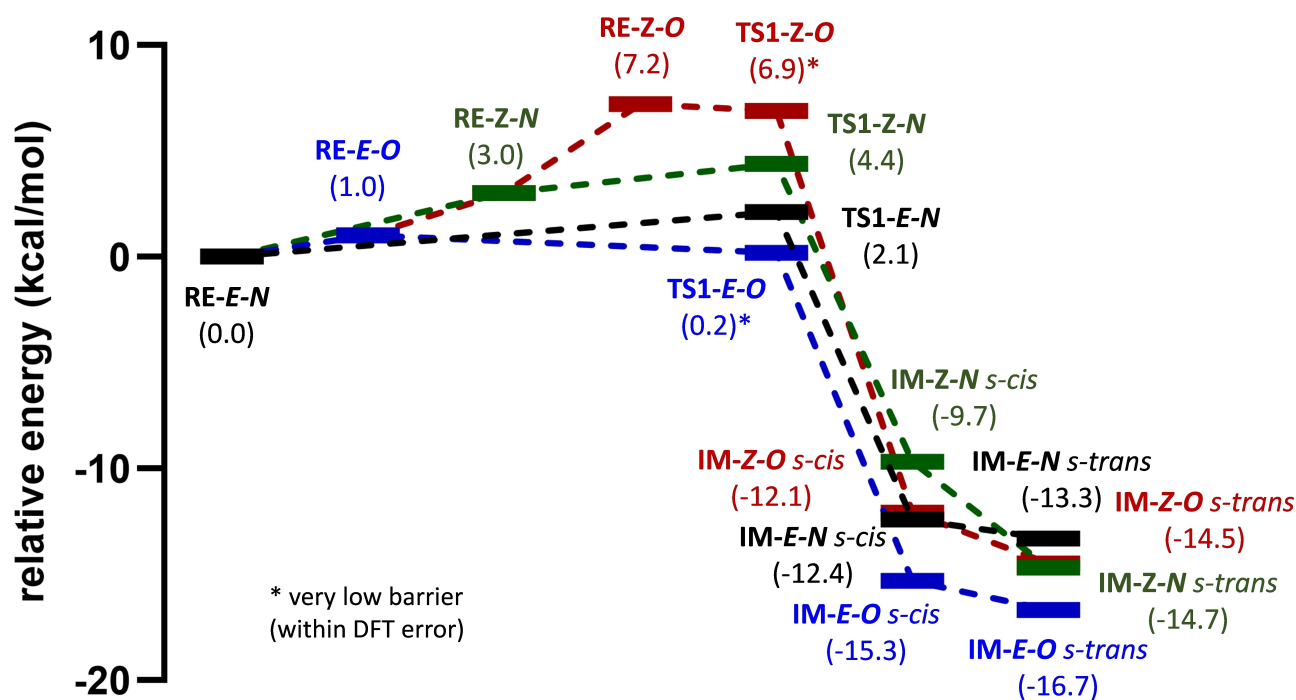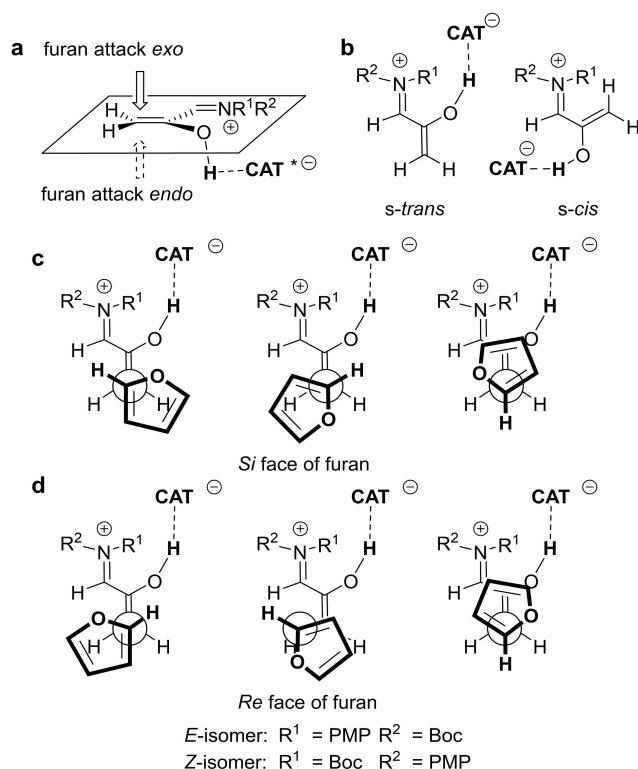

Figure 2. Energy (relative energies given in kcal/mol) profile of the first stage (I).
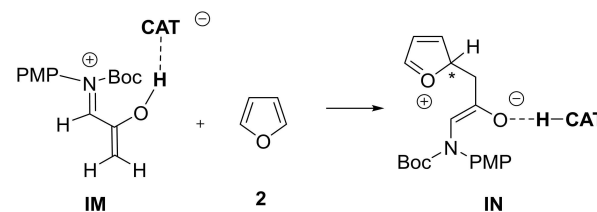
considered the latter for further calculations. The interconversion between *s-cis* and *s-trans* conformers has been calculated to be less than 1.8 kcal/mol which, according to the Curtin-Hammett principle can be considered irrelevant when compared with the reaction barrier. On the other hand, the presence of the oxygen atom makes the *E/Z*-configured iminium ions to be in equilibrium, and therefore both *E* and *Z* isomers will be considered. We also studied the four possible diastereomeric approaches between furan and the oxy eniminium species **IM**, considering three staggered orientations. Additionally, the two coordination modes were taken into consideration, resulting in a total of 48 transition structures (see Figure 3 and SI).

All the transition structures were located, and they converged to a total of 33 optimized transition structures. The best calculated transition structure from each eniminium isomer led to four transition structures that account for 100% according to a Boltzmann distribution (Figure 4).
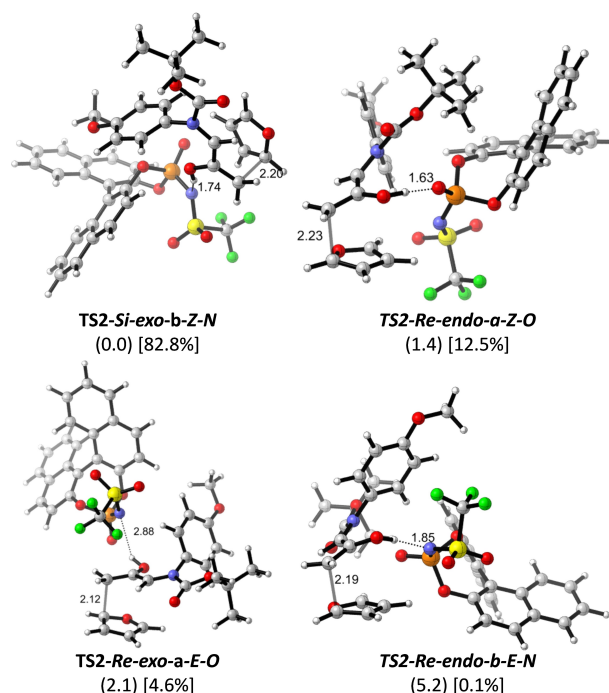
The reaction was studied through the corresponding IRC analysis, which confirmed that the transition

Scheme 6. Reaction between **IM** and furan.

TS2-*Si-exo-b-Z-N* (0.0) [82.8%]
TS2-*Re-endo-a-Z-O* (1.4) [12.5%]
TS2-*Re-exo-a-E-O* (2.1) [4.6%]
**TS2-*Re-endo-b-E-N*** (5.2) [0.1%]

Figure 4. The preferred transition structures representing the two different approaches for the reaction between furan **2** and eniminium **IM**.

Figure 3. Reaction between the oxy eniminium and the furan ring. **a**: Definition of diastereotopic faces of eniminium. **b**: *s-cis* and *s-trans* conformations. **c** and **d**: Three staggered approaches are shown for the Si (**c**) and Re (**d**) faces of furan C-2. Only one diastereotopic face of the eniminium is shown. *E* and *Z* isomers should be considered as well as two coordination modes of the catalyst rendering a total of 48 transition structures. For the nomenclature employed with the different **TS2** see SI.

structures illustrated in Figure 4 connect the eniminium **IM** with the intermediate **IN**, which was stable enough to be located and optimized in all cases. The stability of **IN** is attributed to its coordination with the catalyst, which prevents the collapse of the alkoxy enamine moiety, thereby maintaining the furan oxonium cation scaffold.

The lowest energy transition structure corresponded to the attack of the *Si* face of furan-C2 by the *exo* face of the (*Z*)- eniminium, the latter remaining coordinated through the nitrogen atom of the catalyst. This approach leads to (*R*)-**IN** intermediate. The other three transition structures correspond to the attack through the *Re* face of furan-C2 leading to the (*S*)-isomer of **IN**. The attack by the *endo/exo* faces of the eniminium species is irrelevant for the enantioselectivity since no stereogenic center is generated at the eniminium carbon. The generation of the two remaining stereogenic centers takes place in the next step and it will be

Adv. Synth. Catal. **2023**, *365*, 1–10   **Wiley Online Library**   5

These are not the final page numbers! ↗↗

conditioned by the preferred face of the eniminium ion intermediate, that is determined at the moment of the addition to the furan, and the (*Z*)-configuration of the aminoenolate, that is determined by the *s-trans* conformation of the starting complex. For these reasons, this step is considered the enantiodifferentiating one. The corresponding energy profile is illustrated in Figure 5. Thus, since the process is not reversible (inverse barrier is almost 4-fold the direct barrier: 11.8 vs 4.4 kcal/mol, respectively) we decided to focus on the use of (*R*)-**IN-N**, coming from the most stable transition structure, as the starting point for calculating the next step.

We also calculated this stage for the addition of 2-methylfuran and very similar energy barriers to those observed for furan were obtained (see SI). Consequently, we can asssume (*R*)-**IN-N** as the starting material for the next stage also in the case of 2-methylfuran.
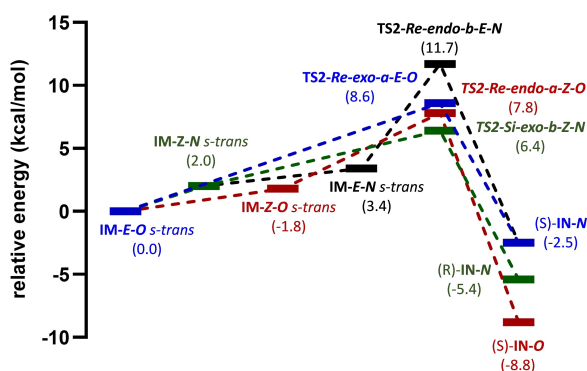
Figure 5. Energy profiles (relative energies given in kcal/mol) for the second stage (II).
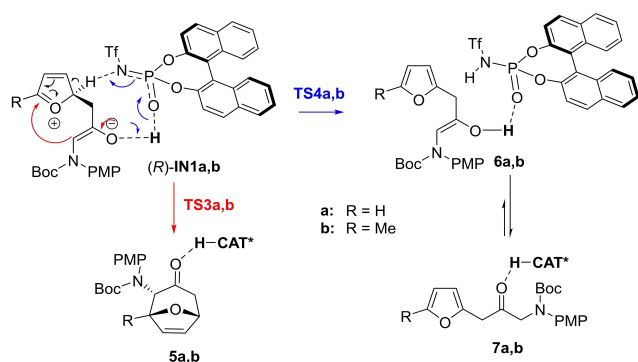
Scheme 7. Formation of products from (*R*)-**IN**. Blue trace corresponds to a typical S_EAr reaction. Red trace reflects the experimentally observed (for R=H) product. **a** and **b** series refer to R=H and R=Me, respectively.
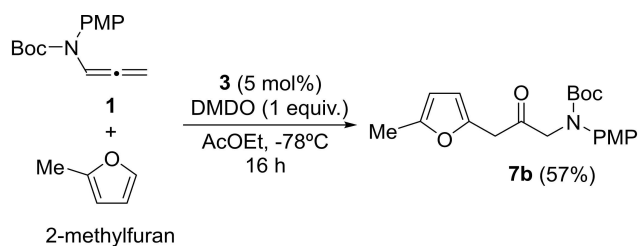
Formation of the Final Products (III)

The intermediate (*R*)-**IN-N** can be seen as a Wheeland intermediate formed from a S_EAr-type reaction of the furan ring in which the eniminium ion acts as the electrophile. The obtention of **5a** is explained by the attack of the enamine-enolate to furan-C4, which can only take place from the same face where the enamine is located (Scheme 7, red trace, R=H), a spatial orientation that has been differentiated in the previous step (Figure 5, green trace).

The transition structure **TS3a** for this step was located after a minimum conformational study, since the configuration defined in the previous step orientates the alkoxy group towards the furan C2 atom. A barrier of 3.9 kcal was been calculated for this step. The alternative completion of the S_EAr reaction, not observed for the situation in which R=H, is the abstraction of the proton by the catalyst to recover the aromaticity of the furan (Scheme 7, blue trace). The abstraction of the proton might be also done by the aminoenolate rendering **7a** directly, but the barrier is considerable higher (see SI). After the proton abstraction event, enol **6a** is formed from which product **7a** is obtained. We also calculated this possibility (**TS4a**), with a barrier of 5.1 kcal/mol, predicting the obtention of **5a** vs. **7a** was obser in excellent agreement with the experimental observation.
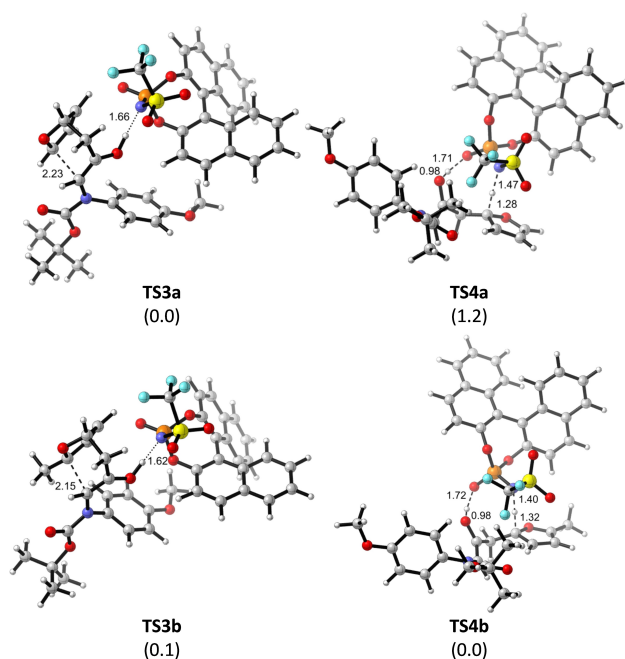
The presence of a substituent at C-2 (not checked in the previous experimental report) could create a stereochemical hindrance rendering the abstraction of the proton more favorable than the attack to a substituted furan-C2.

When we calculated both possibilities for 2-methyl furan (Scheme 7, R=Me) we obtained barriers of 7.6 and 7.5 kcal/mol for **TS3b** and **TS4b**, respectively, predicting that in the case of 2-methyl furan, mixtures of the bicycle **5b** and the achiral compound **7b** should be obtained. The possibility of direct interactions between the catalyst and the iminium ion as reported[14] for a related system were discarded since any attempt of optimizing the corresponding intermediates converged to the coordinated compounds **IM**. This prediction could be confirmed experimentally when compound **1** reacted with 2-methylfuran under the same reaction conditions and compound **7b** was obtained in 57% yield (Scheme 8).

This implies that the first step of the addition had to take place at furan-C5, also demonstrating that the presence of the methyl group prevents the addition also in that stage. In fact, this was also verified experimentally when 2,5-dimethylfuran was evaluated under the optimized reaction conditions, isolating the starting materials (the furan reagent) unchanged. The barriers obtained for the transition structures for this step (Figure 6 and 7) reflect the steric hindrance exerted by the introduction of the methyl group.

Adv. Synth. Catal. **2023**, *365*, 1–10   **Wiley Online Library**   6

These are not the final page numbers! ↗↗

© 2023 The Authors. Advanced Synthesis & Catalysis published by Wiley-VCH GmbH

Scheme 8. Experimental reaction with 2-methylfuran.

Figure 6. Optimized geometries of transition structures leading to final products.
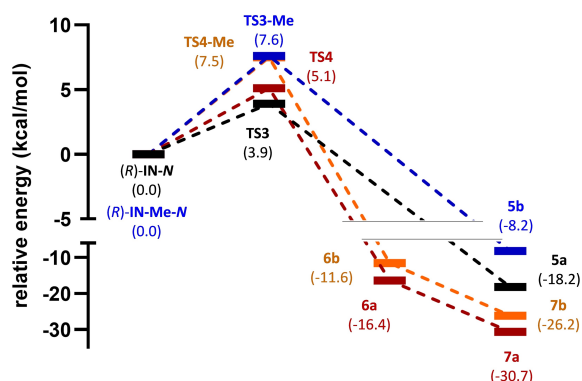
Figure 7. Energy profiles (relative energies given in kcal/mol) for the third stage (III). **a** (black & red) and **b** (blue & orange) series correspond to the reaction with furan and 2-methylfuran, respectively. Black (**a**) and red (**b**) traces correspond to the reaction with furan. Red (**a**) and orange traces (**b**) correspond to the reaction with 2-methylfuran.

Higher values were observed for **TS3b** (3.7 kcal/mol higher than **TS3a**) and **TS4b** (2.5 kcal/mol higher than **TS4a**). The optimized geometries also show unfavorable interactions of the methyl group with the *N*-triflate group of the catalyst in **TS3b**.

The energy profiles for both series are illustrated in Figure 7. Admittedly, the energy differences between **TS3b** and **TS4b** do not justify the sole obtention of **7b** but it should be taken into consideration that for the full study the catalyst has been approached without the two triphenylsilyl bulky groups. Figure 8 illustrates the full process with the three stages for both furan and 2-methylfuran. Whereas the barrier of the rate-limiting steep for the reaction with furan is 6.4 kcal/mol, the value for the reaction with 2-methylfuran is 12.2 kcal/mol as a consequence of the steric hindrance exerted by the methyl group which is close to the reacting site.

To check the validity of the model, we have grown the catalyst to the real one for the rate-determining step. As expected, a higher difference was observed between **TS2-*Re-endo-a-Z-O*** and **TS2-*Si-exo-b-Z-N*** as a consequence of the increased steric hindrance exerted by the triphenylsilyl substituents (Figure 9).

We also studied the diastereoselectivity of the process when substituted allenes were used as substrates (Scheme 1, $R^1 \neq H$). It is assumed that the mere presence of a methyl group does not alter the observed preferred transition structures in the initial stages. Consequently, it is reasonable to assume that the same model is applicable to substituted allenes. We located the preferred transition structure **TS2-*Si-exo-b-Z-N*** for both (*E*)- and (*Z*)-isomers (Figure 10) which can be formed during the ring-opening of the oxirane.

The observed preference for the (*E*)-isomer is in good agreement with the experimental observations (the substituent is *trans* with respect to the amino group), and it is based on steric considerations. An inspection of the model for the unsubstituted allene allows us to conclude that the introduction of an additional methyl at the allenic position should not affect the stereochemical course of the reaction with furan derivative. Therefore, it is expected that the same trend in reactivity with 2-methylfuran will be observed for substituted allenamides.

Conclusion

We have studied the regio-, diastereo- and enantioselectivity for the reaction of allenamides **1** with substituted furans **2** catalyzed by the chiral nonracemic *N*-trifluoromethanesulfonamide **3**. The model using BINOL-derived catalyst correctly predicted all the selectivities, which were mostly dependent on steric factors. This study demonstrates that substitution at C-2 forces the S_EAr-type reaction of furan leading to achiral compounds, but it is necessary, in such a case, to have C5 unsubstituted to allow the first electrophilic

These are not the final page numbers! ⬈⬈
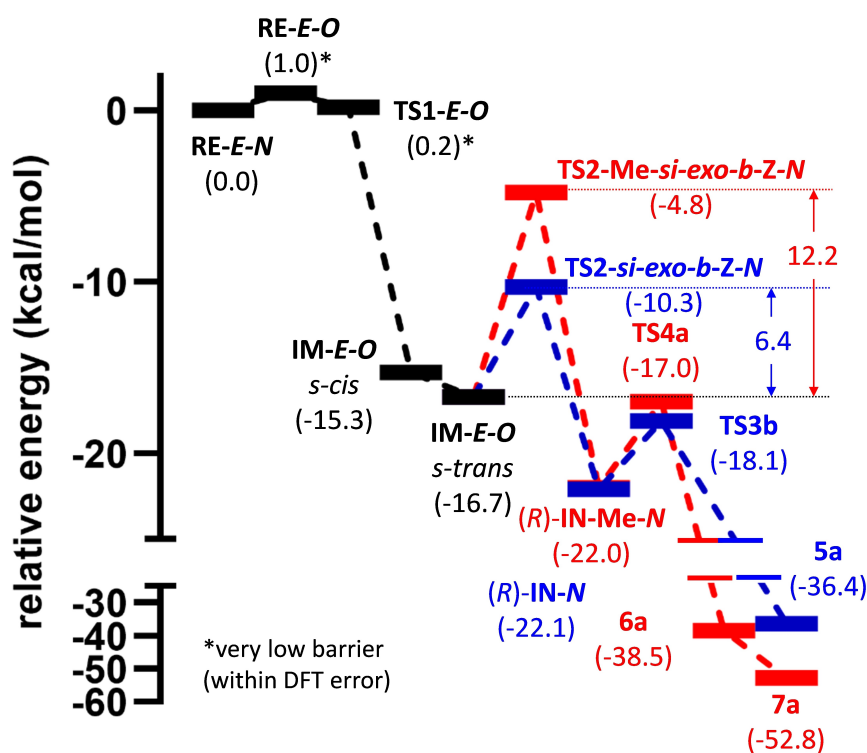
Figure 8. Energy profiles (relative energies given in kcal/mol) for the whole process. Black trace correspond to the common route). **a** (blue) and **b** (red) series correspond to the reaction with furan and 2-methylfuran, respectively.
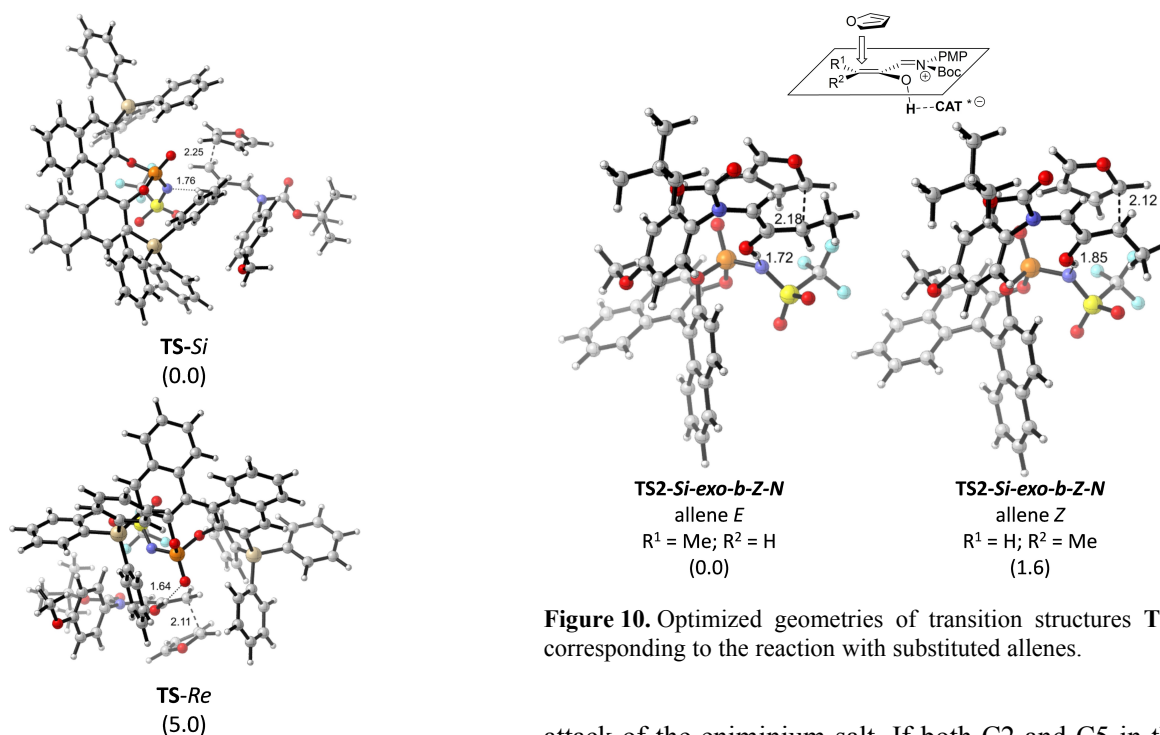
Figure 9. Optimized geometries of transition structures corresponding to the rate limiting step and the real catalyst.

Figure 10. Optimized geometries of transition structures **TS2** corresponding to the reaction with substituted allenes.

attack of the eniminium salt. If both C2 and C5 in the furan ring are substituted there is no reaction. In fact, the reaction with 2-methylfuran showed higher barriers than the reaction with furan and no reaction was observed with 2,5-dimethylfuran.

The rate determining step is the same that the enantiodifferentiating one, i. e. that in which the first stereogenic center is formed (Stage II). The formation of the other stereogenic centers, when the bicycle **5** is obtained, takes place on the same face in which the furan is. Consequently, the attack at furan-C5 is conditioned by the configuration obtained in the previous stage. Nevertheless, the configuration of the amino group ultimately depends on the configuration of an intermediate aminoenolate (*Z* preferred obtained from *s-trans* conformers). The configuration of the allene substituent depends on the *E/Z* preference when the oxirane is formed. In summary, calculations correctly predicted the observed products as well as a behaviour not previously observed that has been demonstrated experimentally in this study.

Acknowledgements

References

[1] S. Kobayashi, K. A. Jørgensen, *Cycloaddition Reactions in Organic Synthesis*; Wiley-VCH Verlag GmbH: Weinheim, Germany, 2002.

[2] a) P. Wipf, Z. Fang, L. Ferrie, M. Ueda, M. A. A. Walczak, Y. Yan, M. Yang, *Pure Appl. Chem.* **2013**, *85*, 1079; b) K. E. O. Ylijoki, J. M. Stryker, *Chem. Rev.* **2013**, *113*, 2244; c) H. Pellissier, *Tetrahedron* **2012**, *68*, 2197; d) A. Moyano, R. Rios, *Chem. Rev.* **2011**, *111*, 4703.

[3] a) X. Yiang, R. Wang, *Chem. Rev.* **2013**, *113*, 5515; b) G. Masson, C. Lalli, M. Benohoud, G. Dagousset, *Chem. Soc. Rev.* **2013**, *42*, 902; c) H. Pellissier, *Tetrahedron* **2009**, *65*, 2839; d) K. C. Nicolaou, S. A. Snyder, T. Montagnon, G. Vassilikogiannakis, *Angew. Chem. Int. Ed.* **2002**, *41*, 1668; e) A. A. Sara, U.-E.-F. Um-e-Farwa, A. Saeed, M. Kalesse, *Synthesis* **2022**, 975.

[4] E. J. Corey, *Angew. Chem. Int. Ed. Engl.* **2002**, *41*,1650.

[5] a) J. Adrio, J. C. Carretero, *Chem. Commun.* **2014**, *50*, 12434; b) J. Adrio, J. C. Carretero, *Chem. Commun.* **2011**, *47*, 6784; c) P. Garner, H. U. Kaniskan, *Curr. Org. Synth.* **2010**, *7*, 348; d) G. Pandey, P. Banerjee, S. R. Gadre, *Chem. Rev.* **2006**, *106*, 4484; e) M. Bonin, A. Chauveau, L. Micouin, *Synlett* **2006**, 2349; f) C. Najera, J. M. Sansano, *Angew. Chem. Int. Ed.* **2005**, *44*, 6272; g) S. Husinec, V. Savic, *Tetrahedron: Asymmetry* **2005**, *16*, 2047; h) I. Coldham, R. Hufton, *Chem. Rev.* **2005**, *105*, 2765.

[6] a) D. A. Foley, R. Maguire, *Tetrahedron* **2010**, *66*, 1131; b) T. V. Nguyen, J. M. Hartmann, D. Enders, *Synthesis* **2013**, 845; c) M. A. Battiste, P. M. Pelphrey, D. L. Wright, *Chem. Eur. J.* **2006**, *12*, 3438; d) F. Lopez, J. L. Mascarenas, *Chem. Soc. Rev.* **2014**, *43*, 2904; e) H. Butenschoen, *Angew. Chem. Int. Ed.* **2008**, *47*, 5287; f) G. Ouvry, *Bioorg. Med. Chem.* **2022**, *57*, 116650; g) B. M. Trost, Z. Zuo, J. E. Schultz, *Chem. Eur. J.* **2020**, *26*, 15354; h) V. Sinka, V. S. Martin, D. A. Cruz, J. I. Padron, *Eur. J. Org. Chem.* **2020**, *2020*, 6704.

[7] For some reviews: a) X. Liu, Y.-J. Hu, J.-H. Fan, J. Zhao, S. Li, C.-C. Li, *Org. Chem. Front.* **2018**, *5*, 1217; b) N. A. Harry, U. S. Mohanan, *Curr. Org. Chem.* **2022**, *26*, 735; c) H. Pellissier, *Adv. Synth. Catal.* **2018**, *360*, 1551.

[8] For some general reviews on (4+3) cycloadditions: a) H. Lam, M. Lautens, *Synthesis* **2020**, *52*, 2427; b) K. Selvaraj, S. Chauhan, K. Sandeep, K. C. K. Swamy, *Chem. Asian J.* **2020**, *15*, 2380; c) H. M. L. Davies, J. R. Denton, *Chem. Soc. Rev.* **2009**, *38*, 3061; d) B. Niess, H. M. R. Hoffmann, *Angew. Chem. Int. Ed.* **2005**, *44*, 26; e) M. Harmata, *Acc. Chem. Res.* **2001**, *34*, 595; f) M. Harmata, *Adv. Synth. Catal.* **2006**, *348*, 2297.

[9] For focussed reviews on (4+3) cycloadditions using oxyallyl cations see: a) A. G. Lohse, R. P. Hsung, *Chem. Eur. J.* **2011**, *17*, 3812; b) M. Harmata, *Chem. Commun.* **2010**, *46*, 8904; c) J. K. Cha, J. Oh, *Curr. Org. Chem.* **1998**, *2*, 217.

[10] a) Z. Yin, Y. He, P. Chiu, *Chem. Soc. Rev.* **2018**, *47*, 8881. For selected reviews on the chemistry and biology of representative compounds with this architecture, see: b) Z. Wu, S. Zhao, D. M. Fash, Z. Li, W. J. Chain, J. A. Beutler, *J. Nat. Prod.* **2017**, *80*, 771; c) A. K. Ghosh, K. Xi, in Natural Products in Medicinal Chemistry, Vol. 60 (Ed.: S. Hanessian), Wiley-VCH, Weinheim, 2014, p. 271; d) M. Saleem, H. Hussain, I. Ahmed, T. van Ree, K. Krohn, *Nat. Prod. Rep.* **2011**, *28*, 1534.

[11] a) M. Harmata, S. K. Ghosh, X. Hong, S. Wacharasindhu, P. Kirchhoefer, *J. Am. Chem. Soc.* **2003**, *125*, 2058; b) J. Huang, R. P. Hsung, *J. Am. Chem. Soc.* **2005**, *127*, 50; c) S. He, R. P. Hsung, W. R. Presser, Z.-H. Ma, B. J. Haugen, *Org. Lett.* **2014**, *16*, 2180.

[12] a) R. P. Reddy, H. M. L. Davies, *J. Am. Chem. Soc.* **2007**, *129*, 10312; b) H. Faustino, I. Alonso, J. L. Mascarenas, F. Lopez, *Angew. Chem. Int. Ed.* **2013**, *52*, 6526; c) I. Alonso, H. Faustino, F. Lopez, J. L. Mascarenas, *Angew. Chem. Int. Ed.* **2011**, *50*, 11496.

[13] a) M. Topinka, K. Zawatzky, C. L. Barnes, C. J. Welch, M. Harmata, *Org. Lett.* **2017**, *19*, 4106; b) J. Ouyang, R. Maji, M. Leutzsch, B. Mitschke, B. List, *J. Am. Chem. Soc.* **2022**, *144*, 8460; c) L. Villar, U. Uria, J. I. Martinez, L. Prieto, E. Reyes, L. Carrillo, J. L. Vicario, *Angew. Chem. Int. Ed.* **2017**, *56*, 10535.

[14] P. Giacinto, A. Bottoni, A. Garelli, G. P. Miscione, M. Bandini, *ChemCatChem* **2018**, *10*, 24421.

Adv. Synth. Catal. **2023**, *365*, 1–10   **Wiley Online Library**   9

These are not the final page numbers! ↗↗

Mechanistic Insights on the Enantioselective (4 + 3) Cycload-dition Between Oxyallylcations and Furans Catalyzed by BINOL-Based Phosphoramides

M. Pedrón*, L. Villar, U. Uria, L. Prieto, T. Tejero, P. Merino*, J. L. Vicario*